Journal of Quantitative Spectroscopy & Radiative Transfer 250 (2020) 106998

Contents lists available at ScienceDirect

Journal of Quantitative Spectroscopy & Radiative Transfer

journal homepage: www.elsevier.com/locate/jqsrt

Multi-wavelength radiometry of aerosols designed for more accurate night sky brightness predictions

Miroslav Kocifaj[a,b,*], František Kundracik[a]

[a] Department of Experimental Physics, Faculty of Mathematics, Physics, and Informatics, Comenius University, Mlynská dolina, 842 48 Bratislava, Slovak Republic

[b] ICA, Slovak Academy of Sciences, Dúbravská Road 9, 845 03 Bratislava, Slovak Republic

ARTICLE INFO

Article history:
Received 12 November 2019
Revised 12 February 2020
Accepted 26 March 2020
Available online 25 April 2020

Keywords:
Aerosols
Size distribution
Optical depth
Night sky brightness
Numerical modeling

ABSTRACT

Scattering by aerosols and gases cause a certain fraction of artificial light emitted upwards is redirected to the ground. Of all atmospheric constituents just the aerosols are most important modulators of night-sky brightness under cloudless conditions. Unlike most of the previous we highlight a crucial role of solar radiometry for determining the atmospheric optical depth before night-time observation is to be made. Aerosol optical depth at visible wavelengths extracted from the data measured provides then the information on size distribution or mean refractive index of aerosol particles that in turn are both necessary to make night sky brightness prediction more accurate. Therefore, combining daytime and night-time radiometry we can achieve accuracy much higher than ever before. This is due to significantly reduced uncertainty in aerosol properties.

The aerosol data are retrieved from a new portable multi-wavelength optical analyzer that operates Ocean Optics spectrometer. The equipment provides the radiance data from 350 nm to 1000 nm with spectral resolution of 1 nm. Due to high sun radiance levels we use a system of mirrors each reducing the signal to about 4%, while keeping the integration time short. The minimum integration time of 3 ms allows for detection of direct sunlight. The system developed is sensitive to small changes in the aerosol system, while showing a good detection limit even under low turbidity conditions. The system performance is demonstrated in field experiment conducted shortly after front passage when most of aerosol particles is effectively removed by rain.

1. Introduction

Aerosols are known to have strong influence on the spectral variation and directionality of the scattered light in a cloud-free atmosphere [12,21,49,53]. Unlike gaseous components, the light scattering by aerosols shows a large asymmetry, and, also the peak intensity in forward direction significantly exceeds that for Rayleigh scattering by air molecules. Therefore, the turbid atmosphere scatters the light more efficiently around the direction of beam propagation. The forward lobe scattering causes the light emitted upwards can propagate to nocturnal environment more easily than light beams scattered uniformly to all directions. The particles small compared to wavelength tend to scatter efficiently to both forward and backward directions while asymptotically approaching Rayleigh scattering pattern. Diversely, the amplitude function for light scattering by a very large particle is derived from the diffraction theory and ruled by Bessel function J_1. The intensity distribution is then proportional to the square of $J_1(x\sin\theta)/(x\sin\theta)$, where $x = 2\pi r/\lambda$ is so-called size parameter. For a spherical particle r is the particle radius and λ is the wavelength of an incident radiation. Unlike Rayleigh theory, the intensity decreases drastically as the scattering angle θ increases. Therefore the size distribution of aerosol particles is a key factor predetermining the angular distribution of scattered light in night-time atmosphere and diffuse illuminance level as a function of distance to the source of light.

Size of aerosol particles ranges from a few hundreds of nanometers (nucleation mode) to several tens of micrometers (coarse mode), while the size distribution function appears to be one of the most variable properties of aerosol systems. Typically urban on-road particles are of sub-micrometer size [18] containing a large fraction of light-absorbing elements, such as carbon or carbonaceous species [11]. Air pollution in an urban area is influenced by local sources (e.g. industry), but wind direction can cause their dominance to be ambiguous. Rural aerosols may differ from urban aerosols in composition, sizes, and/or prevailing morpholo-

* Corresponding author.
E-mail address: kocifaj@savba.sk (M. Kocifaj).

https://doi.org/10.1016/j.jqsrt.2020.106998
0022-4073/

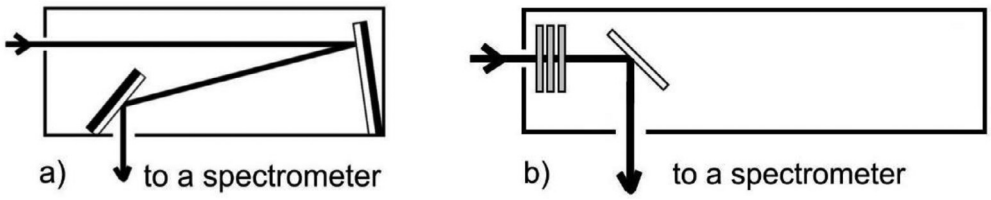

Fig. 1. Optical mounting at the entrance to the spectrometer: (a) optical design with reflecting glassy filters, (b) optical design based on MoC absorption filters.

gies, mostly because of different nature of air pollution sources. Variability of absorption and optical properties of key aerosol types worldwide have been shortly reviewed by Dubovik et al. [16] and the optical effects from single particles and polydispersions are summarized in [35]. No doubt that the night sky brightness (NSB) predictions for urban and rural environments would suffer from inaccuracy when the atmospheric turbidity increases and the information on aerosols is missing.

Optical and physical properties of aerosols are not measured routinely outdoors. Some of the optical data are available from global networks such as e.g. Aeronet, however, monitoring is carried out for only a very limited number of cities. Microphysical properties (including size distribution or chemistry) is scarcely available, while cumulative content of particulate matter 10 μm or less in diameter are obtained by filtration at meteorological stations. In most of cases the aerosol properties are only inferred indirectly, from PM10, visibility, relative humidity etc. [6,32]. The most important are aerosol optical depth, AOD, and number size distribution, $f(r)$. AOD is a measure of atmospheric turbidity and has direct relation to the attenuation of a beam of light on its path in the atmosphere. AOD is also an indirect indicator of light scattering efficiency. The large AOD and more intense scattering are normally detected due to increased aerosol loading. Aerosol optical depth is an integral product of particle size distribution and extinction cross section, so it is not surprising that experimental data of AOD taken at wide range of discrete wavelengths is the vital source of information on $f(r)$. Number size distribution also predetermines intensity distribution for scattered light, thus the methods for concurrent AOD and $f(r)$ retrieval reveal a great potential in achieving a more accurate skyglow predictions.

On overcast nights the fluctuations of NSB amplitude is mostly due to clouds. However, the clear sky radiative transfer surprisingly involves more uncertainty because aerosols of different nature are impossible to distinguish visually although their impacts on skyglow can be large. For instance, the NSB might appear to be moderately graded with a broader light dome over a city or show a steep gradation from zenith toward light source at horizon depending on particle size distribution, while number concentration of particles can remain unchanged. Unlike some meteorological parameters such as cloud coverage, the AOD is the parameter that cannot be deduced from visual sky sighting. An experienced individual observer might be able to distinguish between very bright sky and polluted atmosphere (both observed under cloud-free conditions), but for an accurate quantification we need objective methods and devices. Aerosol-induced changes to NSB can be as large as some orders of magnitude depending on distance to the observer, therefore AOD retrieval is important especially under clear sky conditions.

Basically, the night time aerosol optical measurements are scarce [4,37], while most of them require special conditions and/or devices ([22]; or [34]). This is why we present here a novel alternative to the AOD characterization using portable multi-wavelength solar radiometer that can be used at any site during a day shortly before night-time measurements are to be conducted. The optical system documented in Section 2 is designed for measurements over the visible and near infrared wavelength range aiming to retrieve atmospheric optical depth as a function of wavelength. The inversion routines to compute aerosol properties are analyzed in Section 3, and validated in Section 4 using data acquired during a field experiment.

2. A multi-wavelength atmospheric turbidity analyzer

Wind direction, air pressure field and other parameters are expected to be static or to change smoothly under stable meteorological conditions. The air pressure is high because of large mass of descending air and then days and nights are normally clear. No abrupt changes in the aerosol system are observed thus providing a unique possibility for retrieval of aerosol data in daytime. Two passive methods are commonly used to characterize atmospheric aerosols optically: (1) sun radiometry, and (2) all-sky photometry. The latter ideally requires cloud-free sky or cloud coverage to be very low, and, no cloud masking effects in solar almucantar [52,54] or solar principal plane [36]. The aerosol properties are obtained from radiance data taken at wide range of scattering angles. Due to small angular size of sundisk the good experimental conditions are much easier to achieve for solar radiometry than for all-sky photometry. This increases chances for remote sensing of atmospheric aerosols through unobstructed direct sunbeam measurements [2]. Spectral flux density of solar radiation is also directly related to AOD [3].

A simple concept of multi-wavelength spectrometry allows for routine in-situ atmospheric turbidity analysis at any site. Taking advantage of on-shield projected sun image, its fixation and a special mode in which only the peak intensity is captured, the device we have developed becomes easy to operate manually. No professional system for smooth and precise movement is necessary to point the device toward the sun. The device consists of spectrometer with optical grating and CCD detector sensitive to visible and near infrared wavelengths [31]. Control signal communication and data transfer are made via USB port. Due to its extremely high intensity the sunbeams need to be attenuated before entering window opening at the spectrometer. Even with minimal exposure time of 1/3000 s the signal is still much above the upper detection limit, thus we used neutral filters with transparency of ca 0.2% to avoid signal saturation. Two filter-controlled optical designs are possible: one based on reflection from microscope slide (Fig. 1a), and other one based on MoC absorption filters (Fig. 1b).

The microscopic glass filters are used to deliver sunlight to pinhole entrance aperture (see Fig. 1a) while the flux density of solar radiation is reduced to only ca 0.2% of its initial value. This is due to 4% reflection efficiency attributed to the first reflection event and 5% efficiency for second reflection at the incidence angle of ca 45°. In Fig. 1b sunlight initially passes through a set of three filters made from a thin layer of MoC on a sapphire substrate and then the light is being reflected from aluminum-coated Si substrate. The transmission coefficients of the filters are 0.115, 0.115 and 0.13 respectively, and the reflection coefficient of the Al mirror is ca 0.92. Therefore the intensity of light is reduced to $0.115 \times 0.115 \times 0.13 \times 0.92 \approx 0.16\%$ of its initial value. Both com-

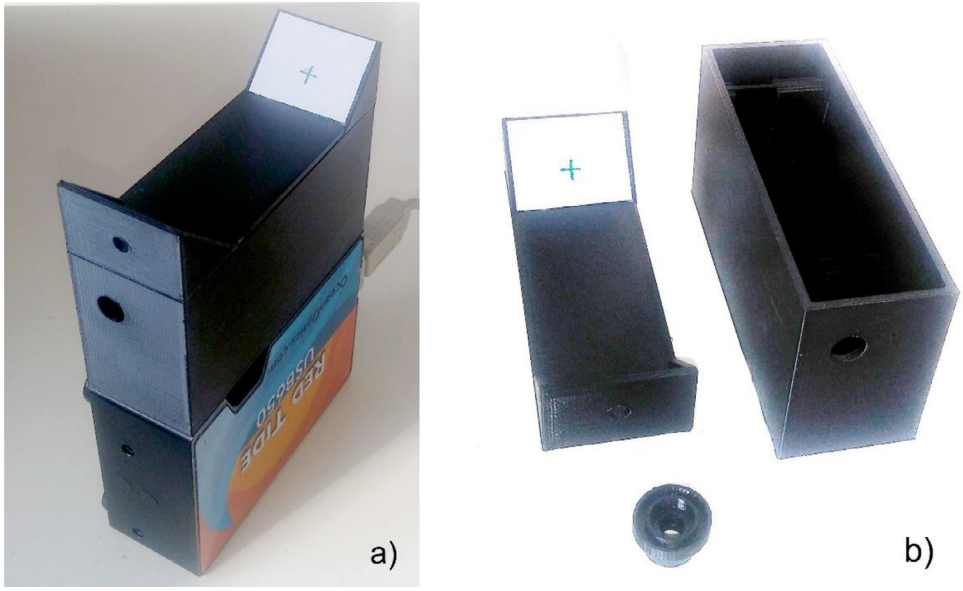

Fig. 2. (a) An atmospheric turbidity analyzer mounting, (b) the system of mirrors, attachment to the spectrometer, and the cover with aiming device, respectively.

ponents can be easily incorporated into a portable device using 3D-printed plastic parts (Fig. 2). The mirrors are fixed in the box, while the attachment has to be screwed to the spectrometer input. The top-element (circular meander) must match the box (light-tight connection). The third part (upper cover) is used as an aiming device.

We have developed platform-independent Java solution to capture solar spectrum and to communicate to spectrometer via OmniDriver controller. First the dark spectrum is taken and the noise is properly digitized also for very low intensity levels. Aiming device that consists of a hole in the front of the mounting and a cross displayed on a projection plane allows to direct the atmospheric turbidity analyzer towards the sundisk. Solar spectrum is captured three times a second and corrected for "hot" pixels (the average of two signals from neighboring pixels is used). Each time the peak-valued spectrum is detected an acoustic signaling is used before new data-set is recorded. Sunlight is so intense that the useful signal level is achieved in a short integration time. It should be noted that each value is the average of 30 measurements, and the spectroradiometer handles a few values per second.

3. Processing of visible and near IR spectra, while obtaining the aerosol properties

Under clear sky conditions the spectral intensity of an extraterrestrial source of light decays exponentially with increasing optical air mass, M. By definition M is proportional to the optical path length in a light scattering medium. For horizontally homogeneous stratified atmosphere illuminated from above by parallel sunbeams the optical air mass can be expressed as follows [10]

$$M(z) = Ch(z) = \sqrt{\frac{\pi R}{2H}}\left[1 - \mathrm{erf}\left(\sqrt{\frac{R}{H}}\cos\left(\frac{z}{2}\right)\right)\right]\exp\left[\frac{R}{H}\cos^2\left(\frac{z}{2}\right)\right], \tag{1}$$

where $Ch(z)$ is Chapman function calculated for an observer at the ground surface, $erf(\ldots)$ is the error function [39], R is radius of the Earth (≈6371 km), H is the atmospheric scale height (≈8 km in accordance with [51]), and z is the observational zenith angle. In Eq. (1) $M(z)$ is zenith-normalized optical air mass, so $M(0)$=1. Many approximations to the above formula exist. Of all, we can introduce M expressed as a function of elevation angle $h = {}^{\pi}/_{2} - z$ [56]

$$M(h) = \frac{2.0016}{\sin h + \sqrt{\sin^2 h + 0.003147}}\,. \tag{2}$$

Eq. (2) is advantageous for applications where the optical phenomena above the horizontal are of key importance. At night when a bright dome of light is observed over a distant city, M is normally required for large values of z, so we prefer Eq. (2). At horizon the optical air mass asymptotically approaches the value of 35.7, meaning that the horizontal optical trajectory in the atmosphere is 36-times the vertical optical path length. On the other hand, to keep the error margin of sunlight measurements low, we normally require M to not exceed the value of 3 (the values above 3 are acceptable under very stable optical conditions). The day-time experiments are therefore limited to $h > 20°$. In such case, $M(z)$ can be approximated by $\cos^{-1}(z)$. The spectral flux density of direct solar radiation measured by the device is

$$I_\lambda(z) = I_{0\lambda} e^{-\tau(\lambda)/\cos z}, \tag{3}$$

where $I_{0\lambda}$ is the instrument's extraterrestrial constant. This means we do not require $I_{0\lambda}$ is to be physically measured in $\mathrm{Wm^{-2}nm^{-1}}$. Uncalibrated values are acceptable, however, we require I_λ to scale linearly with amplitude of optical signals. A constant (C) to convert the device-specific intensity to a calibrated one is not necessary because C cancels out when atmospheric optical depth is computed as follows

$$\tau(\lambda) = \cos z\; ln\left[\frac{CI_{0\lambda}}{CI_\lambda(z)}\right] = \cos z\; ln\left[\frac{I_{0\lambda}}{I_\lambda(z)}\right]. \tag{4}$$

Aerosol optical depth $\tau_A(\lambda)$ (or AOD regularly used throughout this paper) is then obtained by subtracting gaseous-components from $\tau(\lambda)$, i.e.

$$\tau_A(\lambda) = \tau(\lambda) - \tau_R(\lambda) - \tau_{O3}(\lambda) - \tau_{H2O}(\lambda) - \tau_{TG}(\lambda), \tag{5}$$

where $\tau_R(\lambda)$, $\tau_{O3}(\lambda)$, $\tau_{H2O}(\lambda)$, and $\tau_{TG}(\lambda)$ are the optical depths for Rayleigh scattering, ozone absorption, water vapor absorption, and trace-gases absorption, respectively. The contribution from other than above components are negligibly small. Visible and near-infrared spectra of τ_R, τ_{O3}, and τ_{H2O} are shown in Fig. 3 for the standard atmosphere ([19], τ_{TG} is also low compared to other components thus not displayed). Fairly largest contribution to $\tau(\lambda)$

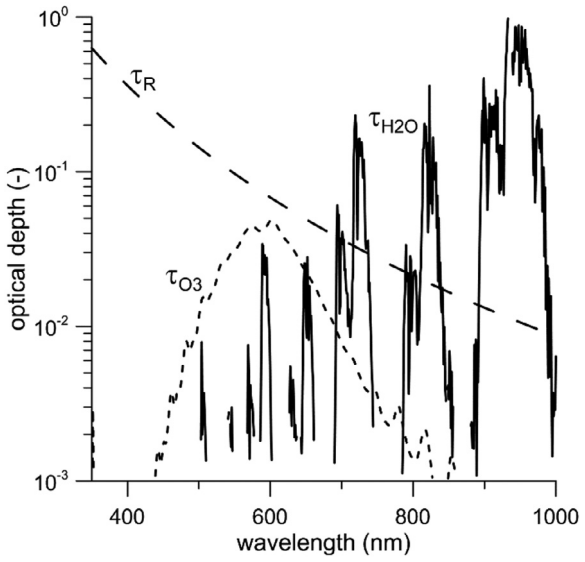

Fig. 3. Optical depths of the most important atmospheric constituents (except for aerosols).

from Rayleigh scattering is found for visible wavelengths, while water vapor absorption dominate all other components in the near infrared.

Light absorption and scattering by aerosol particles cause the flux density of solar radiation would drop significantly in the visible spectral range. Light scattering removes a certain amount of electromagnetic energy from the incident radiation and redistributes the light to both forward and backward hemispheres. Unlike light scattering by aerosols, the absorption is a wavelength-selective process and strongly depends on material composition. For instance, carbon particles [1] and other carbonaceous species [42] typically absorb visible light orders of magnitude more efficiently than mineral particles [26] or some other inorganic constituents ([33] and references therein). Optical depth of aerosol particles is therefore difficult to express analytically or to compute as a fixed function of wavelength. The scattering efficiency of an aerosol particle depends on its size, morphology, chemistry and also on how the material constituents are internally mixed [30]. High sensitivity of $\tau_A(\lambda)$ to the aerosol microphysical properties makes their retrieval from experimental data possible. The most commonly extracted aerosol property is the number size distribution, $f(r) = dn/dr$, with n being the volume concentration of aerosol particles (m^{-3}) and r the particle radius. The function f is so-called columnar size distribution, otherwise also called column-integrated distribution of particles, or the distribution of particles per unit cross section of atmospheric column. It is very common in atmospheric radiometric measurements to deal with columnar size distributions [41]. Normally there is a lack of information on the spatial distribution of aerosols, but Yang and Gordon [55] have shown that effect of aerosol horizontal inhomogeneity generally produces low errors in most of aerosol retrievals (e.g. the error margin for single scattering albedo retrieval from optical remote sensing is less than 1%).

For non-spherical particles the value of r is computed as the radius of volume-equivalent sphere. The contribution to $\tau_A(\lambda)$ from a system of equally-sized particles is obtained as the product of n and $C_{ext}(\lambda)$, where C_{ext} is the cross section for extinction [7]. Therefore, AOD for a population of aerosol particles is obtained as a superposition of all elementary contributions from all particles, i.e.

$$\tau_A(\lambda) = \int_0^\infty C_{ext}(r,\lambda)\ f(r)\ dr\ . \tag{6}$$

For non-spherical particles $C_{ext}(r,\lambda)$ can be computed numerically using the volume integral equation method (such as e.g. Discrete Dipole Approximation; [15]) or extended boundary condition method (e.g. T-matrix; [25]). The latter is more efficient for bodies of revolution [35]. The exact solution to electromagnetic scattering by particles of spherical geometries is known as Mie theory [23] for which a number of approximations exist. Of all, the anomalous diffraction theory attracted a lot of attention [17]

$$Q_{ext}(r,\lambda) = \frac{C_{ext}(r,\lambda)}{\pi r^2} = \frac{2m-1}{m}\left[2 - \frac{4}{y}\sin y + \frac{4}{y^2}(1-\cos y)\right], \tag{7}$$

where Q_{ext} is dimensionless efficiency factor for extinction, m is the complex refractive index of aerosols, and $y = 2x(m-1)$, and $x = 2\pi r/\lambda$ is the size parameter. Due to its analytical formulation the anomalous diffraction theory has been frequently used in particle sizing applications in the past [8,9]. These methods profit a lot from reduced functional dependency of $Q_{ext}(r/\lambda)$ that belongs to a class of product-type kernels.

Retrieval of particle size distribution function $f(r)$ from experimentally determined $\tau_A(\lambda)$ is an ill-posed task, but for the product-type kernels (Eq. (7)) a straightforward procedure exists for determining $f(r)$. We use Mellin's transform of the kernel $Q_{ext}(r/\lambda)$ that is based on two-sided Laplace's transform [29]. It has been shown by Shifrin [44] that inverse kernel has the simple analytical form of $[1-\cos y]/y - \sin y$ for homogeneous non-absorbing spheres. Solution to the integral Eq. (6) then does not increase computational burden because $f(r)$ is a simple one-dimensional integral representation of experimental data function while modulated by inverse kernel. However, the above approach may fail if applied to particles of arbitrary properties, so we rather prefer to find the true solution by minimizing the following functional

$$\Phi_\alpha = \sum_{i_\lambda=1}^{N_\lambda}\left[\sum_{j_r=1}^{N_r} C_{ext}(i_\lambda, j_r) f(j_r) - \tau_A(i_\lambda)\right]^2 + \alpha\left\{\boldsymbol{f}^T\cdot\boldsymbol{H}\cdot\boldsymbol{f}\right\} \tag{8}$$

where N_λ and N_r are the number of measurements and number of discrete radii for which $f(r)$ is to be determined. The indices i_λ, j_r float within defined grid range. The last term is interpreted as a quadratic constraint aiming to penalize large norms of $\boldsymbol{f} = (f_1, f_2, \cdots f_{N_r})$. There is no relation between elements of the density function, so $\boldsymbol{H}$ is a near-diagonal matrix, whose form depends on how the vector $\boldsymbol{f}$ is to be smoothed. The regularization parameter α is to weight the smoothing functional and its proper choice is crucial toward finding realistic solution to $f(r)$. Solution to Eq. (8) is known as Tikhonov's regularization [45] with algorithms described by Press et al. [39] or Twomey [47]. A common approach is to find the solution vector from the following two equations

$$\boldsymbol{f} = \left(\boldsymbol{C}_{\boldsymbol{ext}}^T\boldsymbol{C}_{\boldsymbol{ext}} + \alpha\boldsymbol{H}\right)^{-1}\boldsymbol{C}_{\boldsymbol{ext}}^T\boldsymbol{\tau}_{\boldsymbol{A}}, \tag{9}$$

$$\left|\boldsymbol{C}_{\boldsymbol{ext}}\boldsymbol{f} - \boldsymbol{\tau}_{\boldsymbol{A}}\right|^2 \le \varepsilon^2 \tag{10}$$

where $\boldsymbol{C}_{\boldsymbol{ext}}$ is $N_\lambda \times N_r$ matrix whose elements are scattering cross sections for a specific particle radius (r) and wavelength (λ), $\boldsymbol{C}_{\boldsymbol{ext}}^T$ is the transposed matrix of $\boldsymbol{C}_{\boldsymbol{ext}}$, $\boldsymbol{\tau}_{\boldsymbol{A}} = (\tau_{A1}, \tau_{A2}, \cdots \tau_{AN_\lambda})$ is data vector, and ε is the margin for experimental error. Eq. (10) is to guarantee the true solution satisfies the measure of goodness. In practical applications, especially when $\boldsymbol{C}_{\boldsymbol{ext}}$ does not guarantee the stable solution, experimentation with several distinct kernels can become meaningful. Most typically we reformulate Eq. (6) as follows

$$\tau_A(\lambda) = \int_0^\infty \frac{C_{ext}(r,\lambda)}{\pi r^2}\left[\pi r^2 f(r)\right] dr, \tag{11}$$

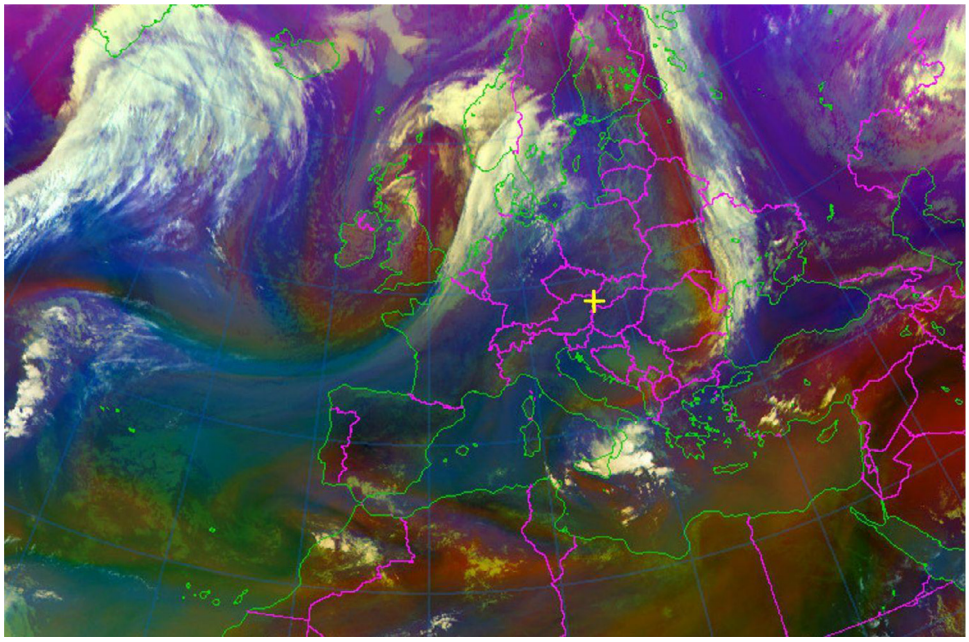

Fig. 4. Meteorological situation for central Europe on Sep. 4, 2019 shortly after front passage (after www.shmu.sk). The field experiment has been conducted in Bratislava (see yellow cross).

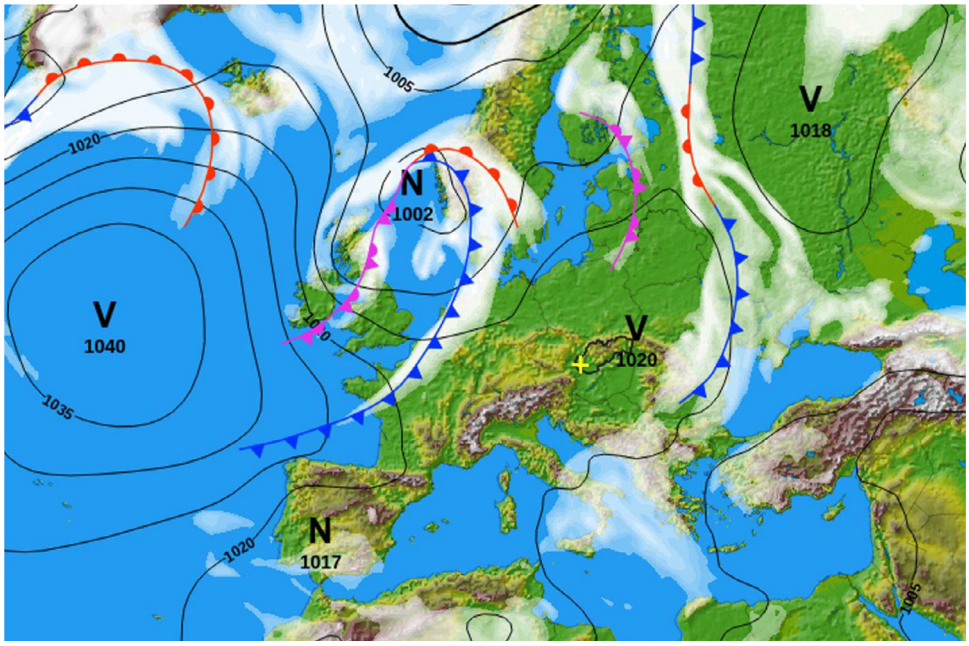

Fig. 5. Air pressure field for central Europe on Sep. 4, 2019 (after www.shmu.sk). The observation point is indicated with yellow cross.

where the new kernel $Q_{ext}(r,\lambda) = \frac{C_{ext}(r,\lambda)}{\pi r^2}$ may appear useful in some retrievals (see [9] for more detail analysis). The sought function is then $s(r) = \pi r^2 f(r)$.

4. Testing the device and validation the model in a field experiment

The device developed is intended to operate under wide range of clear-sky conditions of which the most serious are those when atmosphere exhibits minimal aerosol loading. Extremely low aerosol content causes that the right-hand-side of Eq. (5) quickly approaches zero, thus increasing the error in aerosol optical depth retrieval. Therefore, an arbitrary small imperfection in experimental data can lead to relatively large perturbations of $\tau_A(\lambda)$ and size distribution of aerosol particles as well. Accuracy of aerosol characterization would normally improve as the turbidity increases, therefore we have validated our model shortly after front passage, i.e. under fairly the worst situation when the aerosols were efficiently removed from atmosphere and τ_A was expected to be very low.

The meteorological situation during field experiment on 4.9.2019 is documented in Fig. 4, while the air pressure field is shown in Fig. 5. These meteorological maps demonstrate that the measurements were made under very stable clear sky atmospheric conditions and the air mass extends thousands of kilometers from the position of measuring site (see yellow cross). The spectral flux

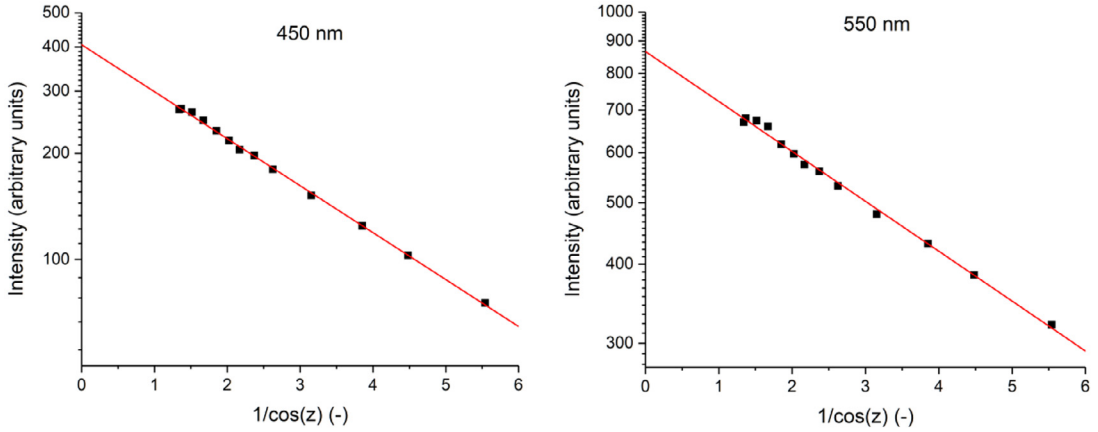

Fig. 6. Signal level at two discrete wavelengths vs. optical air mass. The data were recorded by turbidity analyzer on September 4, 2019 and are shown in arbitrary units on a logarithmic scale.

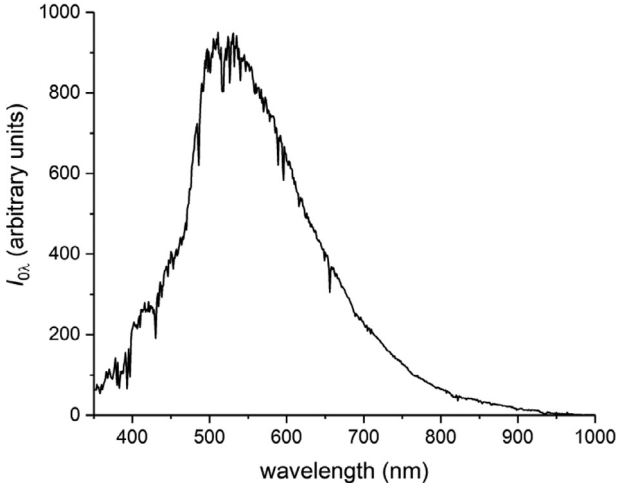

Fig. 7. Instrument-specific extraterrestrial constant $I_{0\lambda}$ as a function of wavelength.

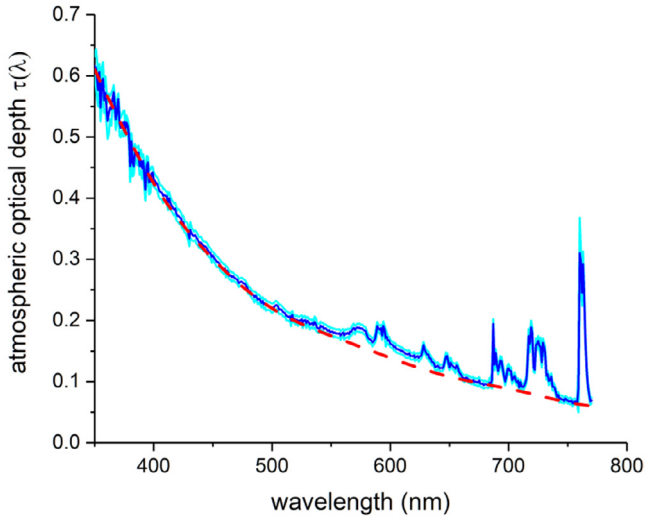

Fig. 8. Atmospheric optical depth $\tau(\lambda)$ as determined on September 4, 2019, in Bratislava (Slovakia). The dark blue line is for average spectrum of $I_{0\lambda}$, while light-blue lines are for minimum and maximum values of $I_{0\lambda}$ obtained within error margin of measuring device. The dashed red line is for continuum due to superposition of $\tau_A(\lambda)$ and $\tau_R(\lambda)$.

density of direct solar radiation has been taken in Bratislava (Slovakia) in the afternoon from 1:27 PM to 7:23 PM of the Central European Summer Time (UTC+2). Under stable optical conditions the logarithm of I_λ should be a linear function of optical air mass, and this is proven in Fig. 6 for two discrete wavelengths, while similar graphics can be drawn for all visible wavelengths.

It follows from Eq. (3) that the slope of a linear function in Fig. 6 changes proportionally with $\tau(\lambda)$. Daily dynamics of atmospheric turbidity typically results in a certain deviation from the linearity. As a consequence, some data are scattered around a line that is the best linear fit to all experimental data. Very clean atmosphere therefore represents an ideal tool for obtaining the instrument's extraterrestrial constant. The technique to determine $I_{0\lambda}$ is known as Langley plot method and uses linear extrapolation of measured data to M=0 (lower limit of x-axes in Fig. 6). It has to be understood that the spectrum of $I_{0\lambda}$ is an instrument-specific property and need not be the same for two different physical devices. Different mountings or filters may result in different $I_{0\lambda}$ as a function of wavelength. For our device $I_{0\lambda}$ is shown in Fig. 7. The ripple structure of solar spectrum is also seen in $I_{0\lambda}$, but some small fluctuations can appear due to momentary optical instability, e.g. turbulence in boundary layer of the atmosphere.

Experimentally determined atmospheric optical depth is documented in Fig. 8 as a function of wavelength. The sharp peaks in red edge of the visible spectrum are due to oxygen and H_2O and should be subtracted from $\tau(\lambda)$ when obtaining $\tau_A(\lambda)$ from Eq. (5). Except for the selective absorption, the scattering spectra of $\tau_A(\lambda)$ and $\tau_R(\lambda)$ dominate all other effects thus resulting in a continuum shown in Fig. 8 as dashed red line. All spectral signatures exceeding the continuum level are due to absorption by gaseous constituents, while all other effects are phantom phenomena due to signal fluctuation or experimental errors and should be eliminated. This is why the further analysis is limited to bounded interval from approximately 420–440 nm to less than 770 nm.

Using Eq. (5) and applying data filtering as mentioned above we have found nearly inverse relationship between τ_A and λ (black squares in Fig. 9). The decline rate of τ_A is often expressed in terms of power law $\approx \lambda^{-\delta}$, where δ is Ångström exponent (see e.g. [46]). In our case $\delta \approx 0.9$ which is a very common value for sub-micrometer-sized particles. Note that Ångström exponent 2 or more indicates the presence of very small particles, while $\delta < 1$ is for large dust or see salt particles (for observations made in maritime regions; [43]). We used Tikhonov's regularization Eqs. (9) and (10) and Mellin transform to retrieve $f(r)$ and found that most of

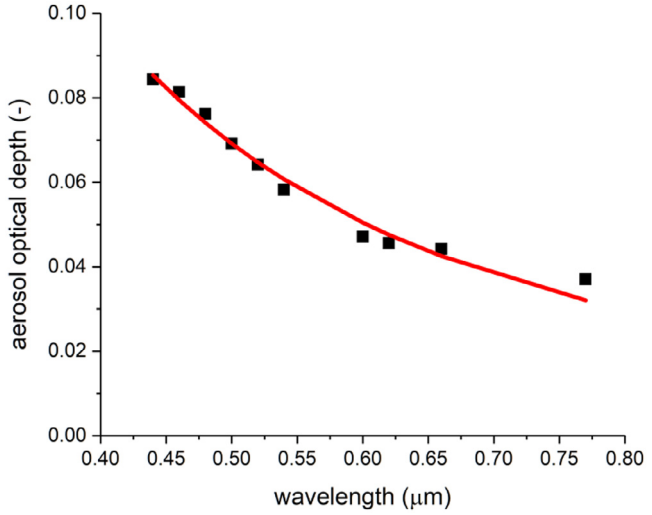

Fig. 9. Theoretical aerosol optical depth (solid line) that best matches data (black squares) experimentally determined on September 4, 2019 in Bratislava (Slovakia).

the particles have radii smaller than 0.4 μm (left plot in Fig. 10). The second mode has been identified with both methods at about 0.9 μm and is more apparent for $rf(r)$ (see right-plot in Fig. 10). The latter is normally the output from Mellin's transform [44]

$$rf(r) = \frac{1}{\pi^2}\int_0^{\infty}\left[\frac{1-\cos(ry)}{ry} - \sin(ry)\right]\left(\frac{y}{2}\right)\left\{\tau_A\left(\frac{y}{2}\right) - \tau_A(\infty)\right\}\, dy, \tag{12}$$

with $y = 4\pi(m-1)r_0/\lambda$ and r_0 being an arbitrary linear scale such as the mode of the number size distribution (see also Sec. Analytical method in [50]). The scale parameter r_0 is arbitrary, but once picked is must be held constant. To integrate Eq. (12) aerosol optical depth should be known for all wavelengths, however, this is generally impossible because radiometers can only operate over a limited wavelength range. Applying the anomalous diffraction theory the asymptotic formulae can be find to simulate $\tau_A(\lambda)$ outside instrument's detection spectral window. For this we have used Eqs. 13a and 13b in [28]. It is demonstrated in Fig. 10 that size distributions of sub-micrometer-sized aerosols obtained from both Tikhonov's regularization and Mellin's transform are nearly identical, but number concentrations of large particles differ. This is not surprising as anomalous diffraction theory is the relevant theory for refractive index approaching unity, although its validity is extended to $m \to 2$ [48]. So even if y is large and fixed, the theory requires the refractive index of particles to approach that of host medium (air). Therefore we expect $rf(r)$ derived from analytical model (12) should be used to only estimate approximate size distribution. Coincidentally, Tikhonov's regularization and Mellin's transform produce similar results, primarily because the refractive index m found from minimizing the functional Φ_α (Eq. (8)) is the real value close to 1.4. The imaginary part of m is undetectably low, so we expect that the air contained non-absorbing particles. The applicability of Mellin transform to such particles has been validated in our early study in 1994 [27]. In further we inserted regularized solution to Eq. (6) in order to test how good the size distribution reproduces the aerosol optical depth measured. There is no doubt that modeled $\tau_A(\lambda)$ matches that of observed profile (compare solid line against black square symbols in Fig. 9). In addition the AOD below 0.09 at visible wavelengths is consistent with very low values of PM_{10} (ranging from 10 to 20 μg/m^3) as measured by the Slovak Hydro-meteorological Institute in September 4, 2019. The method is therefore suitable to characterize aerosol on a local scale and thus allow for more accurate modeling of light pollution propagation into ambient environment at night.

4.1. Concluding remarks

In spite of the great progress in development of methods for measuring night sky brightness [20] and establishment of ground-based monitoring networks in a few countries [5,14,38,40] the geographical coverage of routine night sky imaging stations is still extremely low, and most of data is not collected systematically. Therefore, the theoretical models and numerical methods are (and still remain) irreplaceable and indispensable tools for predicting NSB at arbitrary place and under arbitrary turbidity conditions. Although a portable device is useful for *in-situ* NSB quantification during a targeted field campaign, it is impossible to make such experiments everywhere and at all the time. Therefore, the numerical modeling serves to benefit light pollution community through theoretically well-founded night sky brightness prediction, especially for very isolated places or locations where experimental data are generally unavailable.

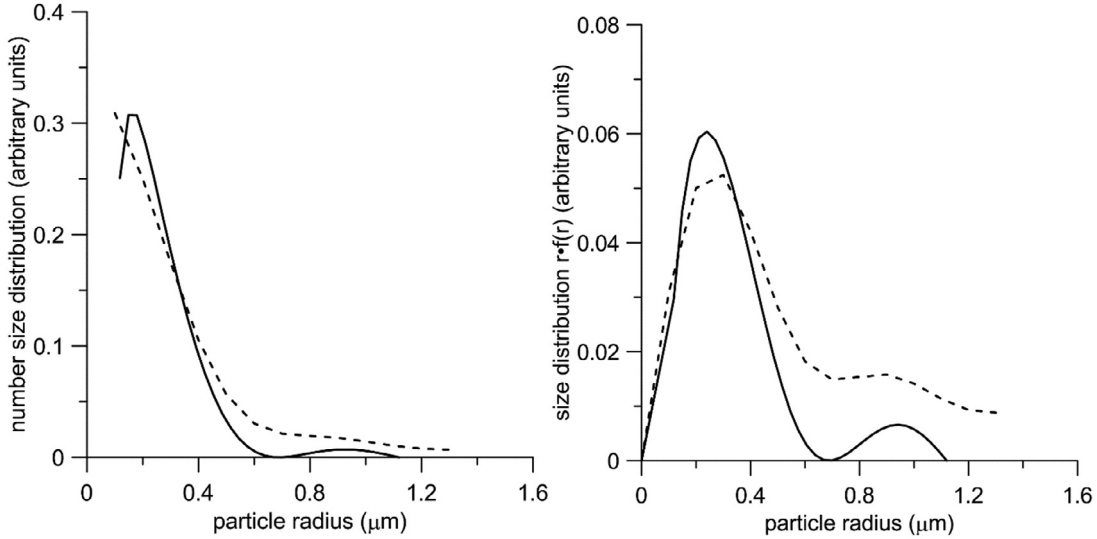

Fig. 10. Left plot: Columnar number size distribution $f(r)$ retrieved from regularization technique (solid line) and Mellin transform (dashed line). Right plot: the same but for $rf(r)$.

NSB can vary over wide range depending on aerosol content and microphysical properties of aerosol, such as aerosol optical depth and size distribution. The latter is decisive in shaping the scattering phase function, $p(\theta)$, which is the probability that photons are directed to angle θ after scattering in an atmospheric environment. It is therefore quite clear that phase function predetermines the angular distribution of diffuse light in a site, and, drastic changes of $p(\theta)$ can have large impacts on NSB gradation, especially at low angular distances to the light sources. The larger particles, the more pronounced forward scattering relative to that backward or sideward scattering. Forward scattering from very small particles is double of that sideward scattering, but $p(\theta)$ for particles large compared to the wavelength can vary over several orders of magnitude when θ floats within its defined range. The information on the number size distribution of aerosol particles, $f(r)$, is therefore extremely important in making more accurate predictions of NSB. It has to be understood that aerosol optical depth τ_A at a specific single wavelength λ^* is not sufficient to qualify and quantify NSB properly because different $f(r)$-functions can produce the same value of $\tau_A(\lambda^*)$. To determine $f(r)$ we either need to inspect AOD as a function of wavelength, or to gather as much as possible *a-priori* information on aerosols to derive $f(r)$ indirectly.

In the paper the method for determining aerosol properties from sunlight measurements is presented, while $\tau_A(\lambda)$ and $f(r)$ determined under stable meteorological situation (nearly static air pressure field) serve as inputs to numerical tool for predicting the night sky brightness at the site of interest. We have shown that inversion of $\tau_A(\lambda)$ is possible using different methods even under low turbidity conditions that are worst for identification of a specific aerosol contribution to the atmospheric optical depth. The Tikhonov's regularization and the Mellin transform are coherent in reproducing both the main peak and the position of subsidiary mode of particle size distribution, but Mellin approximation is limited in range of its applicability. We suggest to use regularization technique whenever is possible, while using Mellin transform for quick estimate in localities with air pollution sources producing primarily non-absorbing or slightly absorbing particles (e.g. sea salt, ammonium sulfate, water, sodium chloride, montmorillonite). The error analysis is in general difficult for the inverse methods, but the accuracy of the size distribution information obtained from optical measurements was documented in many studies including those by Dellago and Horvath [13] and Horvath and Dellago [24].

Author contributions

MK led the project, developed the method to retrieve aerosol properties from sunlight measurements, and performed computations. FK developed and built multi-wavelength atmospheric turbidity analyzer, and conducted the experiments. MK and FK wrote the paper, and analyzed data.

Declaration of Competing Interest

None.

Acknowledgements

This work was supported by the Slovak Research and Development Agency under Project No. APVV-18-0014.

References

[1] Alexander DTL, Crozier PA, Anderson JR. Brown carbon spheres in East Asian outflow and their optical properties. Science 2008;321:833–6.
[2] Alexandrov MD, Lacis AA, Carlson BE, Cairns B. Remote Sensing of Atmospheric Aerosols and Trace Gases by Means of Multifilter Rotating Shadowband Radiometer. Part I: retrieval Algorithm. J Atmos Sci 2002;59:524–43.
[3] Alados-Arboledas L, Lyamani H, Olmo FJ. Aerosol size properties at Armilla, Granada (Spain). Q J R.Meteorol Soc 2003;129:1395–413.
[4] Aubé M, Franchomme-Fosse L, Robert-Staehler P, Houle V. Light pollution modelling and detection in a heterogeneous environment: toward a night–time aerosol optical depth retreival method, Atmospheric and Environmental Remote Sensing Data Processing and Utilization: numerical Atmospheric Prediction and Environmental Monitoring. In: Huang Hung-Lung A, Bloom HJ, Xiaofeng X, Dittberner GJ, editors. Proceedings of the SPIE, 5890; 2005. p. 248–56.
[5] Bará S. Anthropogenic disruption of the night sky darkness in urban and rural areas. R Soc Opensci 2016;3:160541.
[6] Bäumer D, Vogel B, Versick S, Rinke R, Möhler O, Schnaiter M. Relationship of visibility, aerosol optical thickness and aerosol size distribution in an ageing air mass over South-West Germany. Atmos Environ 2008;42:989–98.
[7] Berg MJ, Sorensen CM, Chakrabarti A. Brown carbon spheres in East Asian outflow and their optical properties. J Opt Soc Am A 2008;25:1504–13.
[8] Box GV, Box MA. Information content analysis of aerosol remote-sensing experiments using an analytic eigenfunction theory: anomalous diffraction approximation. Appl Opt 1985;24:4525–33.
[9] Box GP, Sealey KM, Box MA. Inversion of Mie extinction measurements using analytic eigenfunction theory. J Atmosph Sci 1992;49:2074–81.
[10] Brasseur GP, Solomon S. Aeronomy of the middle atmosphere. chemistry and physics of the stratosphere and mesosphere. Springer; 2005.
[11] Castro LM, Pio CA, Harrison RM, Smith DJT. Carbonaceous aerosol in urban and rural European atmospheres: estimation of secondary organic carbon concentrations. Atmos Environ 1999;33:2771–81.
[12] Curtis DB, Meland B, Aycibin M, Arnold NP, Grassian VH, Young MA, Kleiber PD. A laboratory investigation of light scattering from representative components of mineral dust aerosol at a wavelength of 550nm. J Geophys Res 2008;113:D08210.
[13] Dellago C, Horvath H. On the accuracy of the size distribution information obtained from light extinction and scattering measurements—I. Basic considerations and models. J Aerosol Sci 1993;24:129–41.
[14] den Outer P, Lolkema D, Haaima M, van der Hoff R, Spoelstra H, Schmidt W. Stability of the nine Sky Quality Meters in the Dutch night sky brightness monitoring network. Sensors 2015;15:9466–80.
[15] Draine BT, Flatau PJ. Discrete dipole approximation for scattering calculations. J Opt Soc Am A 1994;11:1491–9.
[16] Dubovik O, Holben B, Eck TF, Smirnov A, Kaufman YJ, King MD, Tanre D, Slutsker I. Variability of absorption and optical properties of key aerosol types observed in worldwide locations. J Atmospheric Sci 2002;59:590–608.
[17] Franssens G, Maziere MD, Fonteyn D. Determination of the aerosol size distribution by analytic inversion of the extinction spectrum in the complex anomalous diffraction approximation. Appl Opt 2000;39:4214–31.
[18] Gouriou F, Morin JP, Weill ME. On-road measurements of particle number concentrations and size distributions in urban and tunnel environments. Atmos Environ 2004;38:2831–40.
[19] Ch Gueymard. SMARTS2: a simple model of the atmospheric radiative transfer of sunshine: algorithms and performance assessment. Florida Solar Energy Center; 1995.
[20] Hänel A, Posch T, Ribas SJ, Aubé M, Duriscoe D, Jechow A, Kollath Z, Lolkema DE, Ch Moore, Schmidt N, Spoelstra H, Wuchterl G, Kyba CCM. Measuring night sky brightness: methods and challenges. J Quant Spectrosc Radiat Transf 2018;205:278–90.
[21] Hasekamp OP, Landgraf J. Retrieval of aerosol properties over land surfaces: capabilities of multiple-viewing-angle intensity and polarization measurements. Appl Opt 2007;46:3332–44.
[22] Herber A, Thomason LW, Gernandt H, Leiterer U, Nagel D, Schulz KH, Kaptur J, Albrecht T, Notholt J. Continuous day and night aerosol optical depth observations in the Arctic between 1991 and 1999. J Geophys Res 2002;107:4097 D10.
[23] Hergert W, Wriedt T. The Mie theory: basics and applications, 169. Springer Ser. Opt. Sci.; 2012.
[24] Horvath H, Dellago C. On the accuracy of the size distribution information obtained from light extinction and scattering measurements—II. Case studies. J Aerosol Sci 1993;24:143–54.
[25] Kahnert M. Numerical solutions of the macroscopic Maxwell equations for scattering by non-spherical particles: a tutorial review. J Quant Spectrosc Radiat Transf 2016;178:22–37.
[26] Kandler K, Lieke K, Benker N, Emmel C, Küpper M, Müller-Ebert D, Ebert M, Scheuvens D, Schladitz A, Schütz L, Weinbruch S. Electron microscopy of particles collected at Praia, Cape Verde, during the Saharan Mineral Dust Experiment: particle chemistry, shape, mixing state and complex refractive index. Tellus Ser B Chem Phys Meteorol 2011;63:475–96.
[27] Kocifaj M. Relation between the structure of particles of the dispersion layer and its spectral optical thickness in an optically thin environment. Studia geoph. Et geod 1994;38:399–415.
[28] Kocifaj M. Interstellar dust extinction problem: benchmark of (semi)analytic approaches and regularization method. Contrib Astron Obs Skalnaté Pleso 2004;34:141–56.
[29] Kocifaj M, Kómar L. A rapid approximate inversion of extinction data for partially absorbing particles. Optik (Stuttg) 2015;126:4832–6.
[30] Kocifaj M, Videen G. Optical behavior of composite carbonaceous aerosols: DDA and EMT approaches. J Quant Spectrosc Radiat Transf 2008;109:1404–16.
[31] Kundracik F. (2019). davinci.fmph.uniba.sk/~kundracik1/solar_spectrometer/, accessed 8 November 2019.

[32] Malm WC, Day DE, Kreidenweis SM, Collett JL, Lee T. Humidity-dependent optical properties of fine particles during the BigBend Regional Aerosol and Visibility Observational Study. J Geophys Res 2003;108:4279 D9.
[33] Massie ST, Hervig M. HITRAN 2012 refractive indices. J Quant Spectrosc Radiat Transf 2013;130:373–80.
[34] McHardy TM, Zhang J, Reid JS, Miller SD, Hyer EJ, Kuehn RE. An improved method for retrieving nighttime aerosol opticalthickness from the VIIRS Day/Night Band. Atmos Meas Tech 2015;8:4773–83.
[35] Mishchenko MI. Electromagnetic scattering by particles and particle groups. An introduction. Cambridge University Press; 2014.
[36] Olmo FJ, Quirantes A, Lara V, Lyamani H, Alados-Arboledas L. Aerosol optical properties assessed by an inversion method using the solar principal plane for non-spherical particles. J Quant Spectrosc Radiat Transf 2008;109:1504–16.
[37] Pérez-Ramírez D, Ruiz B, Aceituno J, Olmo FJ, Alados-Arboledas L. Application of Sun/star photometry to derive the aerosol optical depth. Int J Remote Sens 2008;29:5113–32.
[38] Posch T, Binder F, Puschnig J. Systematic measurements of the night sky brightness at 26 locations in Eastern Austria. J Quant Spectrosc Radiat Transf 2018;211:144–65.
[39] Press WH, Teukolsky SA, Vetterling WT, Flannery BP. Numerical recipes 3rd edition. the art of scientific computing. Cambridge, New York, Melbourne, Madrid, Cape Town, Singapore, São Paulo: Cambridge University Press; 2007.
[40] Pun CSJ, So CW, Leung WY, Wong CF. Contributions of artificial lighting sources on light pollution in Hong Kong measured through a night sky brightness monitoring network. J Quant Spectrosc Radiat Transf 2014;139:90–108.
[41] Reagan JA, Byrne DM, King MD, Spinhirne JD, Herman BM. Determination of the complex refractive index and size distribution of atmospheric particulates from bistatic-monostatic lidar and solar radiometer measurements. J Geophys Res 1980;85:1591–9.
[42] Schnaiter M, Horvath H, Möhler O, Naumann KH, Saathoff H, Schöck OW. UV-VIS-NIR spectral optical properties of soot and soot-containing aerosols. J. Aerosol Sci 2003;34:1421–44.
[43] Schuster GL, Dubovik O, Holben BN. Angstrom exponent and bimodal aerosol size distributions. J Geophys Res 2006;111:D07207.
[44] Shifrin KS. The study of the properties of matter from single scattering. In: Theoretical and applied problems of light scattering. Minsk: Nauka i Tekhnika; 1971. p. 228–44.
[45] Tikhonov AN, Arsenin VY. Solutions of ill-posed problems. New York: Wiley; 1977.
[46] Toledano C, Cachorro VE, Berjon A, de Frutos AM, Sorribas M, de la Morena BA, Goloub P. Aerosol optical depth and Ångström exponent climatology at El Arenosillo AERONET site (Huelva, Spain).. Q J R Meteorol Soc 2007;133:795–807.
[47] Twomey S. (2002). *Introduction to the mathematics of inversion in remote sensing and indirect measurements*. Dover.
[48] van de Hulst HC. Light scattering by small particles. New York: John Wiley & Sons Inc.; 1957.
[49] Volten H, Muñoz A, Rol E, de Haan JF, Vassen W, Hovenier JW. Scattering matrices of mineral aerosol particles at 441.6nm and 632.8nm. J Geophys Res 2001;106:17375–401.
[50] Walters PT. Practical applications of inverting spectral turbidity data to provide aerosol size distributions. Appl Opt 1980;19:2353–65.
[51] Waquet F, Cairns B, Knobelspiesse K, Chowdhary J, Travis LD, Schmid B, Mishchenko MI. Polarimetric remote sensing of aerosols over land. J Geophys Res Atmos 2009;114:D01206.
[52] Wendisch M, Von Hoyningen-Huene W. Possibility of refractive index determination of atmospheric aerosol particles by ground-based solar extinction and scattering measurements. Atmos Environ 1994;28:785–92.
[53] Wu Y, Gu X, Cheng T, Xie D, Yu T, Chen H, Guo J. The single scattering properties of the aerosol particles as aggregated sphere. J Quant Spectrosc Radiat Transf. 2012;113:1454–66.
[54] Xu X, Wang J. Retrieval of aerosol microphysical properties from AERONET photopolarimetric measurements: 1. Information content analysis. J Geophys Res Atmos 2015;120:7059–78.
[55] Yang H, Gordon HR. Retrieval of the columnar aerosol phase function and single-scattering albedo from sky radiance over land: simulations. Appl Opt 1998;37:978–97.
[56] Gushchin GP. The methods, instrumentation and results of atmospheric spectral measurements; 1988. Gidrometeoizdat, Leningrad (in Russian).